Leading edge profiles for the reduction of aerofoil interaction noise

P Chaitanya * and P Joseph †
University of Southampton, SO17 1BJ Southampton, UK.

L J Ayton ‡
University of Cambridge, CB2 8PQ Cambrdige, UK.

Aerofoils operating in a turbulent flow are an efficient source of noise radiation by scattering vorticity into sound at the leading edge. Much work has been undertaken demonstrating the effectiveness by which serrations, or undulations, introduced onto the leading edge, can substantially reduce broadband leading edge interaction noise. However, most of this work is focused on sinusoidal leading edge serration profiles. In this paper, a family of serration profiles are proposed that are capable of providing significantly greater noise reductions than single-wavelength serrations at optimal conditions. This new family of profiles will be shown to reduce interaction noise through a fundamentally different noise reduction mechanism than conventional single-wavelength profiles. Unlike single-wavelength profiles, which produce a single compact dominant source region per serration wavelength, these new profiles are designed to produce two or more dominant compact sources per serration wavelength of roughly the same source strength, that are separated in the streamwise direction. Since these sources are arranged to be closer together than the turbulence length-scale, they are highly coherent and, at certain frequencies, radiate exactly 180° **out of phase leading to very high levels of noise reduction in the far field. The experimental noise reduction spectra are compared against an analytic model obtained as a solution of the acoustic wave equation using the Wiener-Hopf technique. This is shown to be unable to capture the main features of the noise reduction spectra as the source strength distribution for other profiles are not captured. A simple model has therefore been developed to explain the noise reduction mechanism for these new profiles, based on interference between sources distributed along the leading edge. Good qualitative agreement is obtained with the experimental results.**

*Research fellow, ccp1m17@soton.ac.uk
†Professor, Senior member AIAA, pfj@soton.ac.uk
‡EPSRC research fellow, member AIAA, lja30@cam.ac.uk

Nomenclature

(Nomenclature entries should have the units identified)

a	=	Distance between the adjacent slits for Slitted profile
b, d	=	Slit dimensions of Variable-slit profile
c_0	=	Chord length
f	=	Frequency
F	=	Functional description of the serration
h	=	Half peak-to-root height
h_s	=	Slit height for Slitted-root profile
h_{eff}	=	Effective height
h_{rr}	=	Streamwise distance between sources for Double-wavelength serrations
$k_{1,3}$	=	Streamwise and spanwise wavenumbers of an incident disturbance
l_c	=	Chopped-peak length
λ	=	Serration wavelength
λ_1, λ_2	=	Serration wavelengths for Double-wavelength profile
λ_{rr}	=	Spanwise distance between sources for Double-wavelength serrations
Λ	=	Integral length scale in streamwise direction
Λ_t	=	Integral length scale in transverse direction
M	=	Mach number
p	=	Far-field pressure
PWL	=	Sound Power Level
q	=	Source strength
q_a, q_w	=	Source strength on slit ends
γ	=	Coherence
$r(\omega), s(\omega)$	=	Relative source strengths for slitted profile
S_{qq}	=	Surface pressure cross-spectra
U	=	Axial velocity
u^*	=	Turbulence intensity
ω	=	Angular frequency
ω_0	=	Tuned frequency
ω_Λ	=	Characteristic frequency linked to the turbulence length
w	=	Slit width

W = Radiated sound power for baseline

W_s = Radiated sound power for serrations

x = Streamwise position

y = Spanwise position

I. Introduction

Aerofoils operating in a turbulent flow are an efficient source of noise radiation by scattering vorticity into sound at the leading edge. This noise generation mechanism is common in many industrial applications. For example, with the introduction of increasing bypass ratio turbofan engines, fan broadband noise has become a dominant noise source whereby noise is generated by the interaction between rotor wake turbulence and the leading edge of the downstream Outlet Guide Vanes (OGV). Wind turbines are another important unwanted environmental noise source where the interaction of large-scale atmospheric turbulence interacting with the rotating aerofoil blades is believed to be one of the dominant noise sources, particularly at very low frequencies [1].

A. Single-wavelength

In recent years there has been considerable interest in the use of leading edge (LE) serrations aimed at reducing interaction noise [2–17]. However, most of these papers were focused on single-wavelength serrated leading edge profiles. The noise reduction mechanism of these profiles has been investigated in detail by [6, 10–12, 18–21] and essentially involves a reduction in the source strength everywhere along the serrated leading edge except at the root location. At this location, it has been shown that the source strength per unit edge length is identical to that of a straight edge in [11]. The result, therefore is that a single compact source distribution is produced concentrated at the serration roots whose source strength is equal to that of the straight edge in [12]. The fundamental upper limit on the sound power reduction that can be achieved using single-wavelength serrations has been identified by [12], which was shown to occur at the optimum serration wavelength λ_0, which is a approximately four times the transverse integral length scale Λ_t of the incoming turbulent flow. At this optimum wavelength the reduction in sound power level at any frequency f is given by $\Delta\mathrm{PWL}(f) = 10\log_{10}(fh/U) + 10$, where h is the serration amplitude, U is the velocity.

The influence of length-scale was also studied by [13]. The authors demonstrated the influence of turbulence anisotropy on the performance of sinusoidal leading edge serrations. They showed numerically that small variations in the turbulence length scales in the chordwise and spanwise directions can produce significant changes in the spectral content of the noise sources at the peak and root regions.

Reference [21] used hybrid lattice- Boltzmann/very-large-eddy-simulation method to investigate the effect of sinusoidal serrations applied to the leading-edge of the vanes of a realistic fan stage. The results confirm the lower frequency limit established in [12] for noise reductions of at least 3dB, which shows that the Strouhal number defined

relative to serration amplitude fh/U must exceed 0.2.

B. Alternative leading edge profiles

More recently, alternative leading edge profiles were proposed by [22] and preliminary noise reduction measurements were presented. In this work, three different profiles were investigated: the Double-wavelength profile, a Chopped-peak profile and a Slitted-root profile. These geometries were shown to provide considerably enhanced noise reductions compared to single-wavelength serrations of the same overall amplitude. In this preliminary investigation, the additional levels of noise reduction were attributed to destructive interference between adjacent compact root sources that radiate out of phase by virtue of the time taken for eddies to convect between the streamwise distance between adjacent roots.

A detailed investigation on the performance and mechanism of double-wavelength serrations has been presented previously in [23]. Noise reductions additional to those obtained on a single-wavelength serration of the same amplitude were shown to depend on just the three non-dimensional factors of ω/ω_0, ω/ω_Λ, λ/Λ, where $\omega_\Lambda = U/\Lambda$ and $\omega_0 = \pi U/h_{rr}$ is the frequency at which two adjacent roots radiate 180° out of phase, Λ is the integral length scale and h_{rr} is the streamwise separation distance between adjacent sources.

The factor that limits the performance of double wavelength serrations was shown in [23] to be due to imperfect coherence between sources on adjacent roots arising from the spanwise length-scale of the incoming turbulence. A new family of leading-edge profiles based on the same noise reduction principle of destructive interference between dominant compact sources distributed over the leading edge was therefore proposed that overcomes this limitation. It is based on the introduction of a number of narrow slits at the roots of the leading-edge profiles. A detailed investigation on the performance and noise reduction mechanism of slitted-root profiles has been studied in detail in [24].

An analytical model has recently been developed to predict the noise generated by turbulence interacting with flat plates with arbitrary leading edge profiles, [25]. This model is a solution of the acoustic wave equation. However, a limitation of this approach, recognized by the authors, is that it does not admit vortical solutions. Secondary vorticity has been shown to be present in numerical predictions obtained from solutions of the Euler equations of interaction noise with single-wavelength serrations [26] and slits [27]. The effects of secondary vorticity were demonstrated to be relatively unimportant in the case of single-wavelength profile but essential to explaining the noise reduction mechanism for leading edge slits [25]. This model will be applied in this paper to predict the noise reduction spectra for all the leading edge profiles investigated in this paper in order to assist in the understanding of the noise reduction mechanism.

[28] extends the work in [22] to include two additional profiles. One comprises a number of slits along the leading edge of varying heights with the objective of providing wide-band noise reduction performance. The other is simply a number of narrow slits at the leading edge periodically located along the span. The optimum ratio of slit width to distance between slits is identified and also includes a detailed discussion of the noise control principle.

The purpose of the current paper is to provide a theoretical framework for understanding the noise reduction

mechanism of these various leading edge profiles. This understanding will allow the further development of leading edge profiles. The analytical model of [25] is reviewed and applied to predict the noise reduction spectra of the various leading edge profiles discussed above. The predictions will be shown to be unable to predict the noise reductions additional to those of single-wavelength serrations. A much more simpler model is then developed based on the interference between partially coherent sources distributed along the leading edge. A limitation with this approach, however, is that the source distribution must be known *a priori* from, for example, numerical simulations. Nevertheless, the model allows for the inclusion of complex features such as secondary vorticity which is absent from solutions of the acoustic wave equation.

II. Experimental setup and instrumentation

A. Flat plates leading edge serrations

For economy and ease of manufacture, a comparative study on noise reductions of different leading edge profiles was performed on flat plates situated within a turbulent flow. Justification for the use of flat plates can be found in [12, 23] where the noise reductions on serrated aerofoils were compared against the corresponding reduction on flat plates with only negligible difference between them. The flat plate with a mean chord (c_0) of 150 mm and span of 450 mm was constructed by joining together two 1 mm thick metallic sheets to allow serrated flat plate inserts 2 mm thick to be inserted between them. All corners were rounded and the trailing edge sharpened to eliminate vortex shedding noise. Further details of this flat plate construction can be found in [8].

B. Open-jet test facility and instrumentation

Far-field noise measurements were carried out at the Institute of Sound and Vibration Research's open-jet wind tunnel facility. The wind tunnel is located within the anechoic chamber, of dimension 8 m x 8 m x 8 m. The walls are acoustically treated with glass wool wedges and the cut-off frequency is 80 Hz. The nozzle has dimensions of 150 mm and 450 mm and provides a maximum flow speed of 100 m/s. A detailed description of the wind tunnel, including its characteristics, is presented in [29]. To maintain two-dimensional flow around the flat plate, side plates are mounted to the nozzle exit which also support the flat plate in the flow. The mean leading edge of the flat plate is located 150 mm downstream from the nozzle exit.

In order to prevent tonal noise generation due to Tollmien-Schlichting waves convecting in the laminar boundary layer, and to ensure complete consistency between the different cases, the flow near the leading edge of the aerofoil was tripped to force transition to turbulence using a rough band of tape of width 1.25 *cm* located at 13 cm upstream of the trailing edge of the flat plate, on both sides.

C. Far-field noise measurements

Far-field noise measurements from the flat plate were made using 11, half-inch condenser microphones (B&K type 4189) located at a constant radial distance of 1.2 m from the mid span of the flat plate leading edge. These microphones are placed at emission angles of between 40^o and 125^o measured relative to the downstream jet axis. Measurements were carried for 10 s duration at a sampling frequency of 50 kHz, and the noise spectra were calculated with a window size of 1024 data points corresponding to a frequency resolution of 48.83 Hz.

The acoustic pressure at the microphone was recorded at the mean flow velocities (U) of 20, 40, 60 and 80 m/s. Noise reductions are presented in terms of the Sound Power Level spectra PWL(f) calculated by integrating the pressure spectra over the polar array of 11 microphones using the procedure described in [8]. Sound power level reductions are determined by subtracting the sound power level spectra due to the serrated flat plate from that due to the baseline straight edge profile.

D. Turbulence characterization

A bi-planar rectangular grid with overall dimensions of 630 x 690 mm^2 located in the contraction section 75 cm upstream of the nozzle exit was used to generate turbulent flow that provides a velocity spectrum that is a close approximation to homogeneous and isotropic turbulence at the aerofoil leading edge. However, we emphasize that the condition of isotropy is not a key requirement for predicting the noise radiation but it allows the velocity spectrum at the aerofoil leading edge to be known. The grid was found to generate a 2.5% turbulence intensity and a 8 mm streamwise integral length-scale at 145 mm from the nozzle exit. For homogeneous and isotropic turbulence transverse integral length scale is given in terms of streamwise integral length-scale by $\Lambda = 2\Lambda_t$ ([30]). The streamwise velocity spectra was found to be in close agreement with the theoretical Liepmann velocity spectrum (see Fig. 3 of [12]).

III. Comparison of different serration profiles

In this section we assess the noise control performance of six families of leading edge profiles with the same overall peak-to-root distance with the objective of identifying the most effective geometry for reducing interaction noise, particularly in the low frequency range where conventional single-wavelength profiles perform poorly. These new profiles will be shown to reduce interaction noise through a fundamentally different control mechanism than single wavelength (sinuoisal or sawtooth) profiles (Fig. 1). Each new family is designed to produce destructive interference between two or more compact source regions per serration wavelength. The families of profiles considered in this paper, shown in Fig. 1, are: a) Sinusoidal/Sawtooth b) Double-wavelength; c) Chopped-peak; d) Slitted-root; e) Variable-slit; f) Slitted geometries.

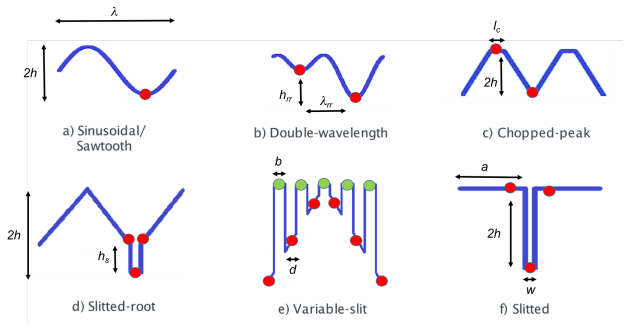

Fig. 1 Schematic of various leading edge profiles considered in this paper and dots indicate dominant sources on the leading edge profiles.

Sound power reductions measured due to the serration profiles investigated in this paper are now compared at roughly the same serration wavelength of $\lambda/c_0 = 0.1$ (except for variable-slit), serration peak-to-root distance $h/c_0 = 0.167$ and flow velocity of 60 m/s. For comparison purposes all the serration families considered in this paper are optimized to achieve best noise reductions whilst maintaining the same wavelength and amplitude. Table 1 summarizes the geometric parameters of each profile, representing the optimum profile obtained from the best noise control performance from more than 150 configurations tested. Also shown in this table is the overall sound power reductions listed in descending order in the frequency range fh/U between 0.1 and 2 corresponding to 240 and 4800 Hz for flow speed of 60 m/s, where most of the energy is contained.

The pure slit case seen to provide best overall noise reductions of 5.2dB due to its better performance at low frequencies. The second and third best performing geometries are the slitted-root and variable slit then followed by the chopped peak and double-wavelength profiles. It is therefore clear that introducing slits provides an effective method to reduce low frequency noise.

A comparison of the sound power reduction spectra for the five optimized profiles are plotted against non-dimensional frequency fh/U in Fig. 2. Also shown for comparison is the sound power reduction spectra for the optimized single-wavelength sinusoidal and sawtooth profiles and also the line, $\Delta\text{PWL}(f) = 10\log_{10}(fh/U) + 10$, which was shown in [12] to provide a close fit to the power reduction spectra for single wavelength profiles at optimum conditions.

The five new profiles clearly provide superior noise reductions at low frequencies ($fh/U < 1$) compared to the single wavelength baseline cases but poorer noise reductions in the higher frequency range ($fh/U \geq 1$).

The most pronounced effect of these new profiles in the low frequency range $fh/U < 1$ is a substantially improved noise reduction performance where the conventional profiles perform comparatively poorly. The noise reduction spectrum from these new families of profiles is characterized by a narrow band peak consistent with the noise control principle of destructive interference between two coherent sources, with each of these sources behaving as a single root source for the case of single-wavelength serrations. These peaks are superimposed on the straight line $\Delta\text{PWL}(f) = 10\log_{10}(fh/U) + 10$, that corresponds to the noise reduction for single wavelength serrations at optimum

Serration profile	dimensions	$\Delta OAPWL$
Slitted	$w/\lambda = 0.13$, $a/\lambda = 0.87$, $\lambda/c_0 = 0.11$	5.16
Slitted-root	$h_s/c_0 = 0.21$, $\lambda/c_0 = 0.1$	4.86
Variable-slit	$\lambda/c_0 = 0.2$, $b/\lambda = 0.13$, $d/\lambda = 0.066$	4.30
Chopped-peak	$\lambda/c_0 = 0.1$, $l_c/\lambda = 0.33$	4.08
Double-wavelength	$\lambda_1/c_0 = 0.067$,$\lambda_2/c_0 = 0.133$, $\phi = \pi/2$, $h_1 = h_2$	3.66
Sinusoidal	$\lambda/c_0 = 0.1$	3.50
Sawtooth	$\lambda/c_0 = 0.1$	3.08

Table 1 Leading edge serration profiles considered in this study for the same peak-to-root amplitude $h/c_0 = 0.167$, OAPWL are calculated for the frequency range of fh/U= 0.1 - 2 where OAPWL for baseline is 76.22 dB at flow velocity of 60 m/s.

conditions [12].

At higher frequencies of approximately $fh/U \geq 1$, these new profiles provide generally poorer noise reductions than single wavelength profiles. The principal reason why noise reductions do not continue to increase with increasing frequency is due to additional noise generated at the trailing edge. Two sources of trailing edge noise have been identified. The first of these is due to the turbulent boundary layer interaction with the trailing edge [8]. Leading edge serration generally causes a thickening of the boundary layer, which is particularly pronounced downstream of the root location [12]. Another source of vorticity passing over the trailing edge has been identified by [26] who has shown through numerical simulation that streamwise vortices generated at the root are a significant source of trailing edge noise. These secondary streamwise vortices are driven by the incoming vorticity. Trailing edge noise, which masks noise reductions at the leading edge, is therefore a balance between naturally generated turbulence in the boundary layer and additional vorticity driven by the incoming turbulence. Overall noise reductions are therefore dependent on the turbulence intensity. The influence of secondary vorticity is particularly significant in the case of pure slits [27] and hence the relatively poor high frequency performance observed in Fig. 2.

Each of the five profiles investigated in this paper are able to reduce far field radiation through a mechanism directly related to the interference between the radiation from sources located on different parts of the profile. Their phase difference is simply governed by their relative streamwise separation distance. However, their main difference is due to their number of dominant sources and their relative frequency-dependent source strengths, which numerical predictions have shown are governed by the presence of secondary vorticity. Especially for chopped-peak and slitted profiles which includes slitted-root, variable-slit and pure slits the source strength is significantly altered. The noise characteristics of each profile is summarized in turn:

Double-wavelength profile: The leading profile of the double-wavelength profile is described by

$$x(y) = c_0 + h_1 \sin(2\pi y/\lambda_1) + h_2 \sin(2\pi y/\lambda_2 + \phi) \tag{1}$$

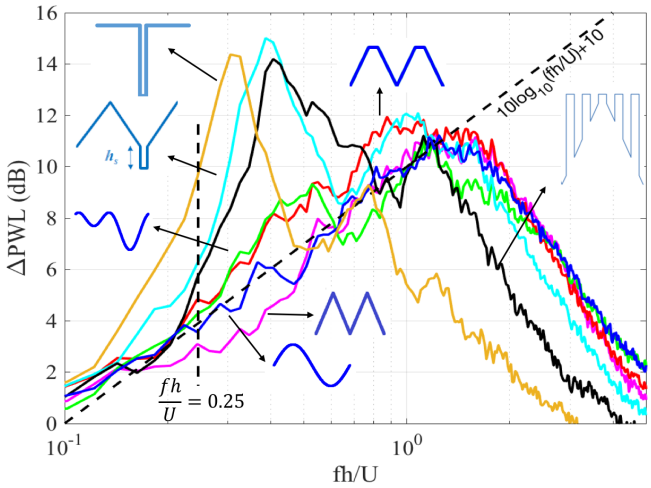

Fig. 2 Acoustic performance of various serration geometries for a fixed peak-to-root distance ($h/c_0 = 0.167$) at flow velocity of 60 m/s (Black dashed: $10\log_{10}(fh/U) + 10$); Blue solid: Sinusoidal; Magenta solid: Sawtooth; Green solid: Double-wavelength; Red solid: Chopped-peak; cyan solid: Slitted-root; Black solid: Variable-slit; Orange: Slitted.

where c_0 is the mean chord, h_1 and h_2 are amplitudes of two single-wavelength components, and wavelengths λ_1 and λ_2 with phase difference ϕ. Of main importance in this design is the streamwise separation distance which determines the frequency ω_0 of maximum noise reductions according to $\omega_0 = \pi U/h_{rr}$, while the spanwise separation distance λ_{rr} determines the degree of coherence between adjacent sources. Note that there is no simple relationship between the parameters in Eq. 1 and h_{rr} and λ_{rr} must be determined by trial and error.

The noise reduction in Fig. 2 for the double-wavelength serration provides an additional noise reduction of 2 and 2.5dB over and above the noise reduction due to the single-wavelength serration. Of all the five serration profiles under consideration the double-wavelength serration has the smallest additional benefit on noise reduction performance. The factors that affect the noise control performance of this profile were discussed in detail in [23] and were shown to be due to the drop in coherence between adjacent source arising from the spanwise separation distance. For this geometry, the peak noise reduction occurs at a non-dimensional frequency of fh/U=0.5, corresponding to fh_{rr}/U=0.64. In the case of the double-wavelength serration, therefore, $h_{rr}/2h = 0.68$. However, one of the advantages of this profile is that the noise reductions at high frequencies are almost identical to those of the single wavelength profiles whereas the slitted profiles discussed below have significantly poorer noise reductions.

Chopped-peak profile: The leading edge profile of the 'Chopped-Peak' simply comprises of a regular sawtooth or single-wavelength profile whose peak is 'clipped'. Clipping the peak has the desired effect of increasing the source strength at the tip with the objective of matching more closely the source strength at the root leading to more effective destructive interference.

The noise reduction spectrum of the Chopped-peak profile in Fig. 2 provides slightly improved noise reductions compared to the double-wavelength serration, especially at high frequencies. As for the double-wavelength serrations, the noise reduction performance of the Chopped-peak serration is ultimately limited by the coherence between the interfering sources. One of the unique features of its noise reduction spectra is the appearance of two non-harmonically related peak frequencies at roughly fh/U=0.4 and fh/U=0.85. The reason for this subtle behaviour will be explained in Section VI.C in terms of interfering coherent sources along the leading edge.

Slitted-root profile: This profile comprises a sawtooth profile in which narrow slits with typical widths of just a few millimetres are introduced at the root positions. The introduction of these slits, upon interaction with turbulent flow, produces two compact acoustic source regions at either streamwise ends of the slit. However, since these sources are aligned in the streamwise direction and the turbulent flow convects along the slit as a frozen pattern, they are highly coherent. By virtue of the time taken for eddies to convect along the length of the narrow slit the sources at either end of the slit destructively interfere more effectively than that of the double-wavelength serration.

The noise reduction spectrum in Fig. 2 shows the appearance of a single peak frequency of maximum noise reduction at fh/U=0.4, which corresponds to $fh_s/U \approx 0.5$, where h_s is the slit height. At this peak frequency, almost 9dB to 10dB of noise reductions are observed additional to those due to single-wavelength serrations. The noise reductions at high frequencies are about 2dB poorer than that of single-wavelength serrations, which appear to represent the best performing leading edge profile in the high frequency range.

Variable-slit profile: The Variable-slit profile is based on the same control principle as the slitted profile except that a number of slits are now introduced of varying slit height with the objective of providing wide-band noise reduction performance. This leading edge profile therefore involves a number of compact source regions radiating with different phases.

The noise reduction spectrum in Fig. 2 can be observed to be effective over a broader range of frequencies than the other profiles that are tuned to a single frequency. However, a maximum noise reduction still peaks at non-dimenstional frequency fh/U=0.4, which can be attributed to interference between two sources at either end of the longest slit. Two further sub-peaks correspond to the interference between two sources at either end of the two shorter slits. These peak frequencies will be explained using a simple model in section VI below.

Slitted profile: The slitted profile simply comprises narrow slits of width w and height $2h$. This design has the combined advantage that the sources are almost perfectly aligned along the streamwise direction, and therefore are highly coherent, and also that they have maximum streamwise separation distance between dominant sources leading to improved low frequency performance.

The noise reduction spectra in Fig. 2 for the purely slitted case has the best low frequency performance with a maximum noise reduction at fh/U=0.3, where additional levels of noise reduction of 10dB are observed. As seen in Table 1 it also has the best overall noise reductions. Also seen in the noise reduction spectra is the first odd harmonic peak frequency of about fh/U=0.8, which provides further confirmation of interference as the main noise control principle.

In summary, all of these profiles provide substantially better noise reductions by up to 10dB at low frequencies compared to conventional single-wavelength or sawtooth serrations. However, in view of the superior performance of the slitted profile, the next section of this paper is dedicated to quantifying and understanding its noise reduction performance.

IV. Slitted leading edge profiles

The principal dimensions of the slitted profile are sketched in Fig. 3, where a and w, the distance between adjacent slits and the slit width respectively, are the two main dimensions controlling noise reduction performance.

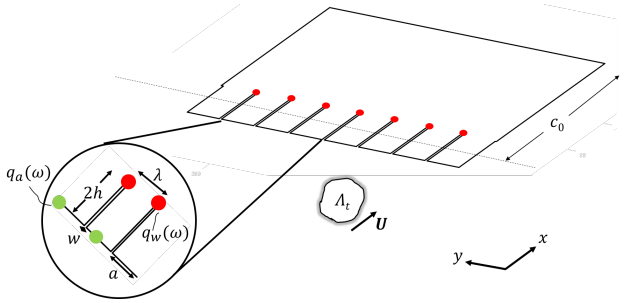

Fig. 3 A sketch of the slitted leading edge serration.

A. Acoustic performance of slitted profiles

To demonstrate the improved effectiveness of slitted profiles compared to single-wavelength profiles the sound power spectra for the baseline flat plate is compared against that for these two profiles of the same height $2h/c_0 = 0.33$ in Figure 4a at a fixed slit width $w = 2.2$ mm at a jet velocity of 60 m/s. Also shown in Figure 4b is a comparison of the directivities at f=720Hz, h=2.5 cm and U =60 m/s, corresponding to $fh/U = 0.3$ where greatest noise reductions are obtained. //

The noise reduction spectra due to the slitted profile can be observed to be significantly higher than that due to the single wavelength serration at $fh/U \approx 0.25$, close to the frequency of $fh/U < 0.3$ where the sound power due to the baseline aerofoil is highest. This slitted profile therefore provides the best overall sound power reductions, as shown in Table 1. At lower frequencies close to $fh/U \approx 0.15$, the noise is dominated by vortex shedding from the turbulence grid. However, the slitted profile provides poorer high frequency noise reductions than the conventional

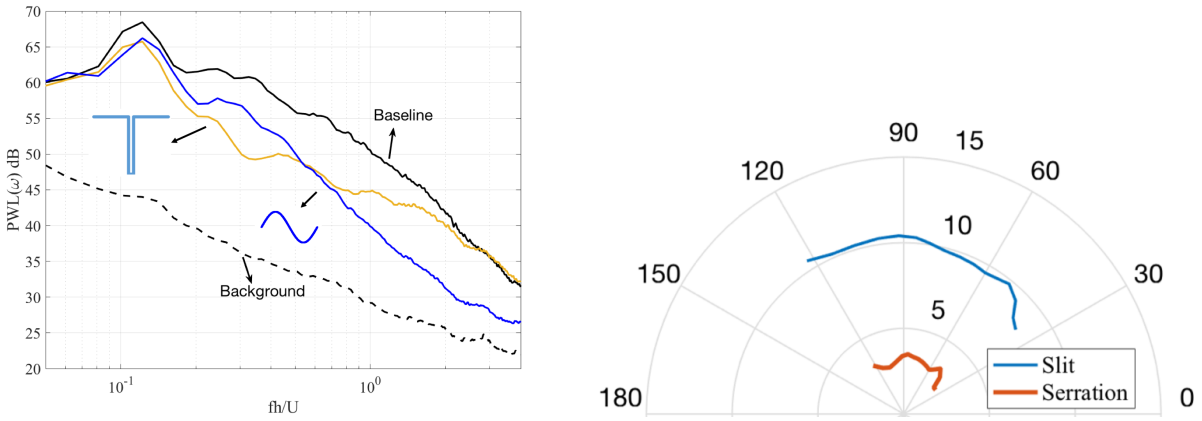

Fig. 4 a) Sound power spectral comparisons for a slitted profile (Orange) for a slit height $2h/c_0$ of 0.33 at a fixed slit width $w = 2.2$ mm and jet velocity of 60 m/s with sinusoidal leading edge (Blue), baseline configuration (Black) and Background noise (Dotted black), b) Noise reduction directivity of slitted and sinusoidal serrations at a fixed non-dimensional frequency $fh/U = 0.3$.

single wavelength profile. Note that background noise is significantly lower than the noise due to the flat plates over most of the frequency range.

The noise reduction directivity is observed to vary by up to 3dB at this frequency over the relatively small range of range measurement angles 40° and 125° compared with 1.5dB for the single-wavelength serration at a fixed frequency of $fh/U = 0.3$. This greater variation in the case of the slit is consistent with stronger interference between the two compact source regions at either ends of the slit. Strong directivity due to slitted profiles is the result of interference between the two sources either ends of the slit, and has been investigated in detail in numerical predictions performed by [27].

We start by assessing the effect of flow speed on the noise reduction performance of slitted leading edge profiles. Figure 5 shows the sound power reduction spectra plotted against non-dimensional frequency $f2h/U$ for a typical slitted profile with a serration amplitude of $h/c_0 = 0.167$, slit width $w/\lambda = 0.13$ (w = 2.2 mm), and $a/\lambda = 0.87$ at the four flow speeds of 20, 40, 60 and 80 m/s. Also shown is the line $10\log_{10}(fh/U) + 10$ representing the optimum sound power reduction achievable for a single-wavelength serration at the optimum wavelength. The sound power reduction spectra for a single-wavelength serration of optimum wavelength [12] is also plotted in Fig. 5 at the flow velocity of 60 m/s.

The slitted profile provides consistently better noise reductions than single wavelength profiles up to a frequency of $f2h/U$=1.5. Above this frequency, however, its performance is worse. The peak frequencies of maximum noise reduction of $f2h/U$= 0.6, 1.5 and 2.5 are entirely consistent with the hypothesis of destructive interference between two dominant compact source regions of roughly equal strength at either ends of the slit, as sketched in Fig. 3. However, the level of noise reduction at these peak frequencies can be seen to be a complex function of the flow speed and hence rms turbulence velocity. At high frequencies, noise control performance progressively worsens as flow speed is increased.

This observation can be linked to strong streamwise vorticity generated along the edge of the slit and interacting with the trailing edge. This secondary vorticity will increase with increasing flow speed leading to increasing levels of trailing edge noise.

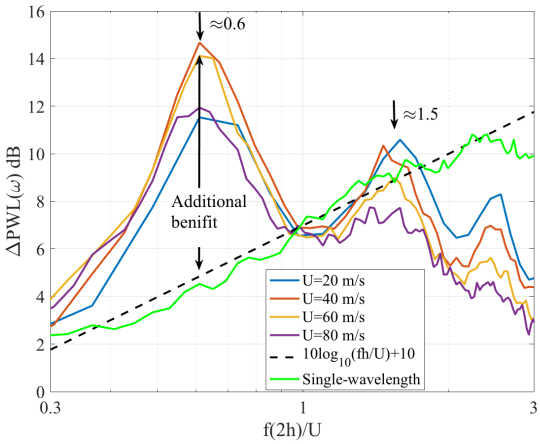

Fig. 5 Influence of jet velocity on noise reduction of slitted serrations of slit width $w/\lambda = 0.13$ and slit height $h/c_0 = 0.167$.

Given that the main noise reduction mechanism arises from reduction of source strength and interference between the sources along the leading edge of length a to sources along the root of length w, we now consider the sensitivity of noise reductions to the ratio of a/w.

B. Optimum slit width

We now consider the noise reduction performance of 35 flat plate serrations consisting of all combinations of 7 slit widths w between 0.7 and 10.3 mm and 5 leading edge widths a between 3 and 30 mm at a fixed slit height of $2h/c_0$=0.33. In Fig. 6 the comparison of the sound power reduction spectra at a fixed slit width of 2.2 mm and a jet velocity of 60 m/s and 5 different values of a corresponding to the width ratios a/w of 1.27, 2.18, 4, 6.72 and 9. A well defined optimum ratio close to 7 (in the cases considered) is observed at this slit width and height. More work is needed to determine the optimum ratio at different slit heights. We note that significant noise reductions (up to 10dB) are still obtained with very narrow slits. This procedure was repeated for the other 6 slit widths. This optimum ratio a/w for each of the 7 values of w considered is tabulated in table 2.

These tabulated results indicate a mean value between 6 to 7 with some small variations at higher slit widths.

Figure 7 shows the comparison of sound power reduction spectra for each of the 7 optimum slit ratios tabulated above at a fixed jet velocity of 60 m/s. The peak noise reduction frequency in the noise reduction spectra shown in this Fig. 7 occurs close to $f(2h)/U \approx 0.6$. As the slit width w is increased, the peak frequency $f(2h)/U$ of maximum noise reduction approaches, from above, a value of approximately 0.5 while the level of maximum noise reduction decreases,

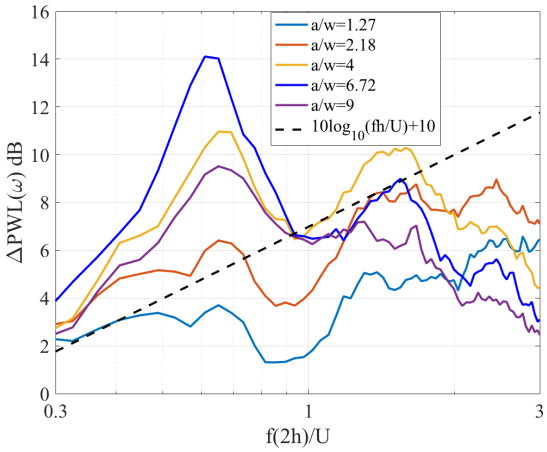

Fig. 6 Sound power reduction comparisons for a slitted profile for varying slit distance a at fixed slit width $w = 2.2$ mm, at jet velocity of 60 m/s.

w (mm)	a (mm)	$(a/w)_{optimum}$
0.7	4.8	6.8
1.2	8.8	7.3
2.2	14.8	6.7
3.2	19.8	6.2
4.3	24.7	5.7
5.3	29.7	5.6
10.3	39.7	3.8

Table 2 Optimum slit width condition for various slit widths for slit height of $2h/c_0 = 0.33$

reaching a level of approximately 7dB (compared to the baseline). Clearly, therefore the acoustic centers of the two sources are not exactly located at either ends of the slit at distance $2h$ but rather at an effective distance h_{eff}. It is possible to formalize this concept by defining h_{eff} to be the effective separation distance for which fh_{eff}/U=1/2, where f is the frequency of the first peak of maximum noise reduction. This may be simply interpreted as the separation distance between two point sources separated by h_{eff} that are out of 180° out of phase at frequency f. The effective centers of the two sources therefore move closer together, tending from above to $2h$ as w is increased. The effect of reducing the streamwise separation distance is to reduce the value of $f2h/U$ towards 0.5, while the effect of reducing spanwise separation distance is to increase the coherence of the two sources and therefore enhancing the level of destructive interference. Best noise reductions are therefore obtained when w is made as small as possible while maintaining the optimum ratio a/w.

C. Influence of slit height on noise reductions

We now investigate the influence of slit height on the noise reductions. Figure 8 shows the comparison of the sound power reduction spectra for the three different slit heights $2h/c_0$ of 0.066, 0.2, 0.33 at a fixed slit width w=1.2 mm

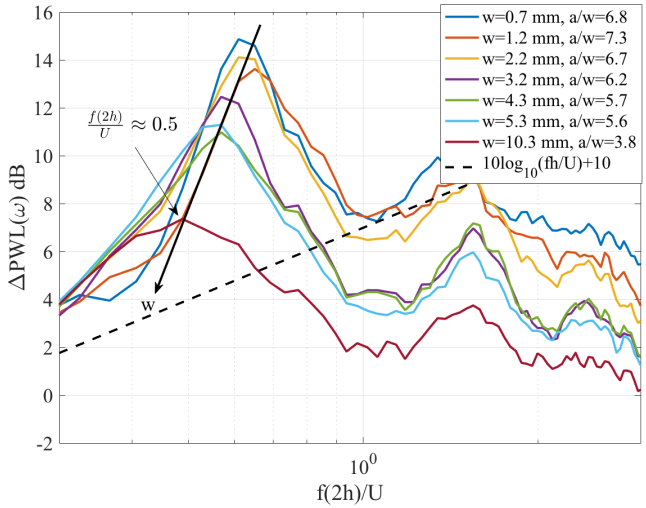

Fig. 7 Sound power reduction comparisons for seven different slitted profile of varying slit width w and at optimum slit dimensions and jet velocity of 60 m/s.

corresponding to the optimum a/w = 6.7 at $2h/c_0$=0.33 and jet velocity of 60 m/s. In this case of fixed slit width, the level of noise reductions is highly sensitive to slit height, with the greatest reductions of up to 14dB occurring for the longest slit. Note that a fairer comparison would involve optimization of the slit width for each slit height.

The peak frequencies $f(2h)/U$ in the noise reduction spectra in Fig. 8 of maximum noise reduction can be observed to increase from 0.5 to 0.65 as the slit height is increased. The precise reason for this observation is currently unclear but is almost certainly due to the variations in the effective source positions with slit height and the frequency-dependence of the two source strengths. More work is needed to understand more clearly the effect of slit width and height on effective source position and source strength.

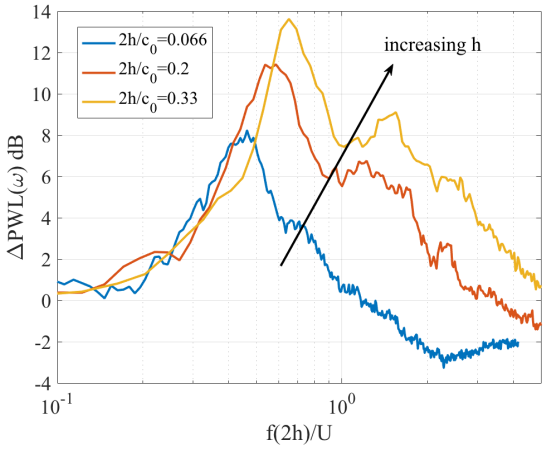

Fig. 8 Sound power reduction comparisons for a slitted profile for three different slit heights $2h/c_0$ of 0.066, 0.2 and 0.33 at a fixed slit width w = 1.2 mm and jet velocity of 60 m/s.

The experimental noise reduction spectra presented above for the various leading edge profiles show complex behaviour containing a number of peaks. In principle, sophisticated analytic and numerical methods could be used to predict the noise reduction spectra for these complex leading edge profiles. However, in the following sections we present a considerably simpler model based on interfering sources along the leading edge that is capable of predicting the main features of the noise reduction spectra, particularly the frequency of peak noise reductions.

V. Analytical model

The previous sections have highlighted the improved noise reduction performance of the leading profiles described above. In an attempt to understand the noise reduction mechanism we first consider the analytic model due to [25] which allows the prediction of the noise radiation due to any arbitrary periodically varying leading edge flat plate profile interacting with a single harmonic vortical gust. Critically, the model is based on the solution to the convected Helmholtz equation with appropriate boundary conditions and therefore does not allow for the presence of secondary vorticity, which is likely to play an important role in the noise reduction of some of these profiles. Full details of the theoretical derivation may be obtained in [25] and key equations are provided in appendix.

The predictions of the noise reduction spectra obtained from this model for the five profiles sketched in Figure 1 for the same measured in-flow turbulence parameters are plotted in Figure 9 and can be compared directly against the experimental spectra in Figure 2.

The predicted sound power level reduction spectra can be observed to be unable to predict the experimental spectra. Whilst the experimental noise reduction spectra show clear evidence for the existence of compact localized sources through the presence of strong interference peaks, no such behaviour is observed in the numerical predictions. Clearly, therefore, these compact source regions are generated through the presence of secondary vorticity which cannot be captured from purely acoustical solutions. Except for the single-wavelength serration, the analytic model [25] is unable to capture the experimental spectra for these optimized geometries where it is believed that the source strength is altered significantly.

VI. Generalised simplified analytical model to predict noise reductions from arbitrary leading edge profiles

Section V has indicated the deficiency of purely acoustic solutions for predicting the noise reductions due to arbitrary leading edge profile interacting with turbulence flow that omit the presence of secondary vorticity. In this section we propose a simple analytical model that assumes that the source distribution is concentrated along the leading edge and is known *a priori*. The simple model cannot therefore predict absolute levels of noise reduction but will be shown below to predict the additional peaks in the noise reduction spectra resulting from interference between different sections along the leading edge whose phase difference is determined from their relative streamwise separation distance.

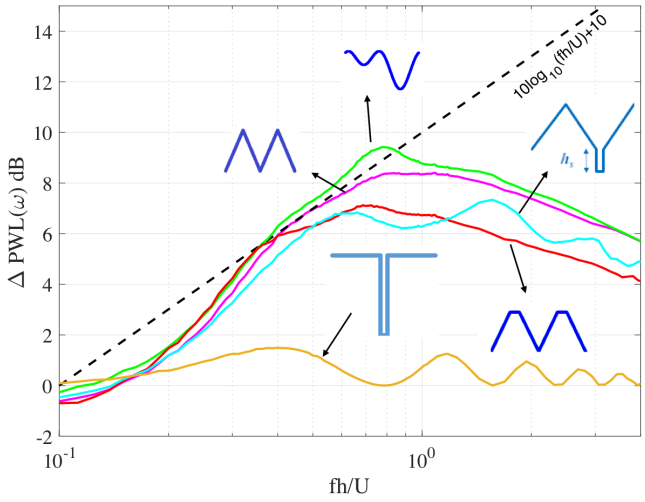

Fig. 9 Analytically predicted acoustic performance of various serration geometries for a fixed peak-to-root distance ($h/c_0 = 0.167$) at flow velocity of 60 m/s (Black dashed: $10\log_{10}(fh/U) + 10$); Magenta solid: Sawtooth; Green solid: Double-Sawtooth; Red solid: Chopped-peak; cyan solid: Slitted-root; Orange: Slitted.

Consider an arbitrary leading edge profile $x = f(y)$, where x is the chordwise distance of the leading edge at any spanwise distance y. In this simplified model we assume that the far field acoustic pressure $p(\omega)$ is simply related to the source strength $q(x, y, \omega)$ integrated over a serration wavelength λ along the leading edge. We further assume that the relative phase difference between each point on the leading edge to the far field noise arises only from difference in time delay taken for the turbulent eddies to convect to the leading edge location x. The source at any spanwise position y therefore has a relative phase difference of $\omega x/U$ so that integrating over the leading edge over one period therefore gives,

$$p(\omega) \propto \int_0^{\lambda} q(x, y, \omega) e^{-i\omega x(y)/U} dy \tag{2}$$

The radiated sound power W_s is related to the mean square far-field pressure integrated over some suitable closed surface,

$$W_s(\omega) \propto \overline{p^2}(\omega) \propto \mathbf{E}[p^*(\omega)p(\omega)], \tag{3}$$

Substituting equation 2 in equation 3, the radiated sound power becomes,

$$W_s(\omega) \propto \int_0^{\lambda} \int_0^{\lambda} \mathbf{E}[q^*(x, y, \omega)q(x', y', \omega)] e^{-i\omega(x'(y') - x(y))/U} dy dy', \tag{4}$$

where $\mathbf{E}[q^*(y, \omega)q(y', \omega)]$ can be recognized as the cross spectrum between any two sources y and y', which may

be further written in terms of the source strength coherence function

$$\mathbf{E}[q^*(x, y, \omega)q(x', y', \omega)] = \sqrt{\overline{q^2}(x, y, \omega)\overline{q^2}(x', y', \omega)}\gamma^2(x, x', y, y', \omega) \tag{5}$$

However, it is reasonable to assume that the incoming turbulence is frozen over the short distance of the serration. In this case, therefore, the coherence is only a function of the spanwise source positions y and y' and hence the dependence on x and x' will be omitted from hereon.

The coherence function $\gamma^2(y, y', \omega)$ between two points y and y' along the leading edge of a flat plate at any streamwise position x from the leading edge can be readily computed from $\gamma^2(y, y', \omega) = S_{qq}(x, y, y', \omega)/S_{qq}(x, 0, \omega)$, where $S_{qq}(x, y, y', \omega)$ is the surface pressure cross-spectrum given in [31, 32].

We now consider the application of this simple model to predict the noise reductions of the various profiles investigated experimentally above and compare against the corresponding measured noise reductions. The first case under consideration is the conventional single wavelength profile.

A. Sinusoidal wavelength: Uniform source distribution

The noise reduction due to conventional single wavelength profiles has been considered by a number of researchers. Its profile is of the form $x = c_0 + h\cos(2\pi y/\lambda)$. We assume here for simplicity that the source strength is constant along the sinusoidal leading edge with source strength $q(\omega)$ and whose coherence between different points along the leading edge is simply a function of the spanwise separation distance relative to the frequency-dependent length-scale $l(\omega)$. The source strength cross spectrum in Eq 4 is now expressed in terms of the coherence function $\mathbf{E}[q^*(y, \omega)q(y', \omega)] = \overline{q^2}(\omega)\gamma^2(|y - y'|, \Lambda_t, \omega)$ where $\overline{q^2}(\omega)$ is the mean square source strength. In order to test the validity of the simple model of Eq. 4 knowledge of γ^2 is required. For the sake of simplicity we assume that this coherence function is identical to that at the leading edge of flat plate. Some justification for this assumption has been presented in [11] and investigated further in [23] which showed that γ^2 along the leading edge was only a function of the spanwise separation distance compared to the turbulence integral length-scale $|y - y'|/\Lambda_t$ and non-dimensional frequency $\omega\Lambda_t/U$.

Noting that $x(y) = h\cos(2\pi y/\lambda)$, the radiated sound power spectrum for single wavelength profiles is of the form

$$W_s(\omega) \propto \overline{q^2}(\omega)\int_0^\lambda\int_0^\lambda \gamma^2(|y - y'|, \Lambda_t, \omega)e^{-ih\omega(\cos 2\pi y/\lambda - \cos 2\pi y'/\lambda)/U}dydy', \tag{6}$$

Using the coherence function estimates derived by [23] in Eq. 6 the sound power radiated by a sinusoidal serration was computed with an amplitude $h/c_0 = 0.167$, wavelength $\lambda/c_0 = 0.167$ at a flow velocity of 60 m/s for five values of turbulence length-scales λ/Λ_t between 3 and 25 . The results was compared against the sound power $W(\omega)$ of a baseline, straight edge case, derived from Eq. 6 by putting $h = 0$.

The sound power level reduction spectra for the five cases are shown in Fig. 10 versus $f(2h)/U$. Also shown for comparison is the semi-empirical line $10\log_{10}(fh/U) + 10$, which corresponds to the optimum wavelength for best performance for single-wavelength serrations as indicated by [12].

The predicted noise reduction spectra in Fig. 10 is observed to oscillate with frequency with an amplitude that reduces as the integral length is reduced. Note that in the limit of $\lambda/\Lambda_t \rightarrow 0$, [12] has shown that Eq. 6 tends to $10log_{10}J_0^2(\omega h/U)$, where J_0 is the Bessel function of the first kind of order 0. Whilst most predictions roughly follow the line $10\log_{10}(fh/U) + 10$ we note that the value of λ/Λ_t that most closely matches the the line is $\lambda/\Lambda_t = 8$, which is significantly higher than the optimum ratio of 4 obtained experimentally. This discrepancy is undoubtedly due to the approximate calculation of the coherence function γ^2 and the assumption of uniform source strength along the leading edge. Nevertheless, being able to capture the general frequency behaviour provides confidence in the simple model. This model will therefore now be applied to the more complex leading edge geometries described above to explain the various additional peaks in their noise reduction spectra.

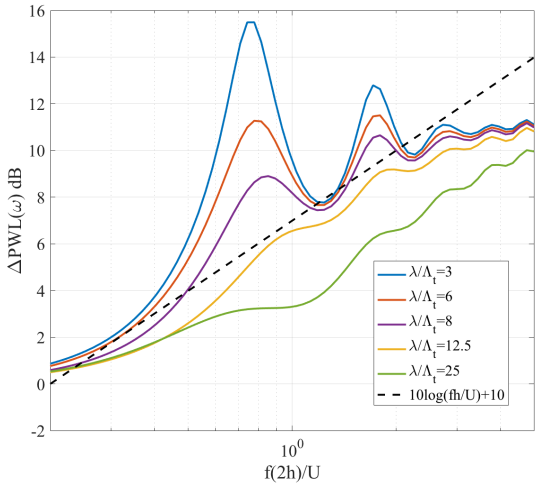

Fig. 10 Predicted behaviour of ΔPWL on λ to validate the single-wavelength noise reduction hypothesis.

B. Slitted leading edge: Two perfect coherent sources of different source strengths

A preliminary analysis of the slitted-root design has previously been presented in [24]. In this section the analysis is extended using the general theoretical framework described by Eq. 4. The most effective serration geometry for reducing interaction noise has been shown in Section IV.A to be narrow slits cut into the leading edge. The noise reduction spectra for this case, plotted in Fig. 2, strongly suggests that the dominant noise reduction mechanism simply involves the destructive interference between two compact, highly coherent sources either side of the slit separated in the streamwise direction by the slit length $2h$. In this case, therefore, the source distribution $q(x, y)$ can be represented as $q(\omega, x, y) = q_a(\omega)\delta(x = 0, y = 0) + q_w(\omega)\delta(x = 2h, y = 0)$, where the slit is assumed to be located at $y = 0$ with the

leading edge at $x = 0$ and the root at $x = 2h$, and δ is the Dirac delta function. Substituting this source distribution into the expression for sound power of Eq.4, performing the integration over the source distribution, and noting that the leading edge and root spanwise locations are identical, $y = y'$, and the coherence function in Eq. 5 must be equal to unity $\gamma^2(0) = 1$, the final expression for the sound power becomes,

$$W_s(\omega) \propto \left[\overline{q_a^2}(\omega) + \overline{q_w^2}(\omega) + 2\sqrt{\overline{q_a^2}(\omega)\overline{q_w^2}(\omega)}\cos(\omega 2h/U)\right]. \tag{7}$$

where $\overline{q_a^2}(\omega)$ and $\overline{q_w^2}(\omega)$ are the mean square source strengths at the frequency ω at the two locations at either ends of the slit. Note that the source strengths q_a and q_w are likely to be complicated functions of the slit width, length and frequency. The reason for the appearance of a strong, highly localized source at the end of the slit has been investigated by Cannard [27] who showed that it was due to the interaction between an intense secondary streamwise vortex generated along the edges of the slit with the root.

The sound power radiation $W_s(\omega)$ from the slitted root serration may now be compared to the baseline straight leading edge $W(\omega)$, whose effective compact source strength is $q(\omega)$. The sound power level reduction compared to the straight leading edge case may therefore be written as,

$$\Delta PWL(\omega) = 10\log_{10}\left(\frac{W(\omega)}{W_s(\omega)}\right) = 10\log_{10}\left(\frac{\overline{q^2}(\omega)}{\overline{q_a^2}(\omega) + \overline{q_w^2}(\omega) + 2\sqrt{\overline{q_a^2}(\omega)\overline{q_w^2}(\omega)}\cos(\omega 2h/U)}\right). \tag{8}$$

Equation (8) for the noise reduction spectrum makes clear that it is completely governed by two source strength ratios. The first, $r(\omega)$, quantifies the relative strengths between the two sources at either ends of the slit,

$$r^2(\omega) = \frac{\overline{q_w^2}(\omega)}{\overline{q_a^2}(\omega)}. \tag{9}$$

The second, $s(\omega)$, quantifies the relative strengths between the source of the un-slitted profile and the sum of source strengths at either ends of the slit,

$$s^2(\omega) = \frac{\overline{q^2}(\omega)}{\left(\sqrt{\overline{q_a^2}(\omega)} + \sqrt{\overline{q_w^2}(\omega)}\right)^2}. \tag{10}$$

The final expression for the sound power level reduction due to a single slit in terms of the ratio of source strengths defined in Equations (9) and (10) is given by,

$$\Delta PWL(\omega) = 10\log_{10}\left(\frac{s^2(\omega)}{1 + \frac{2r(\omega)}{(1+r(\omega))^2}(\cos(\pi\omega/\omega_0) - 1)}\right). \tag{11}$$

where ω_0 is the 'tuned frequency' at which the two sources are exactly 180° out of phase, given by,

$$\omega_0 = \pi U/2h. \tag{12}$$

Equation (11) suggests that noise reductions obtained from the slitted profile compared to the straight leading edge (baseline) are due to two factors. The first is due to a modification in the source strengths between the baseline $q^2(\omega)$ and the slitted profiles $(\sqrt{\overline{q_a^2}(\omega)} + \sqrt{\overline{q_w^2}(\omega)})^2$ as accounted for by the ratio $s(\omega)$. The second factor is due to interference between the two source strengths at either ends of the slit whose effect is quantified by the denominator in Equation (11). This term goes to zero, and hence perfect noise cancellation is predicted, when the source strengths at the either end of the slit at the frequency ω_0 are equal, i.e., $r(\omega_0) = 1$, and radiate exactly 180^o out of phase.

We now assess the validity of the simple two-source model described by Equation (11) to predict the noise reductions for the slitted serration profile, which will then be compared against the experimental noise reduction spectra.

Two slitted profiles are now considered with optimum ratio a/w =6.8 and 5.7 selected from Table 2. They have significantly different slit widths of w=0.7 mm and 4.3 mm with identical peak-to-root distance of $2h/c_0 = 0.33$. The measured noise reduction spectra at a flow speed equal to 60 m/s are plotted against ω/ω_0 and compared in Fig. 11 against the predicted spectra. The values of the source strength ratio $r(\omega)$ were chosen to equal 1.42 and 1.61 to provide the best fit to the measured noise reduction spectra for w = 0.7 mm and 4.3 mm respectively, over the frequency range of interest. Note that, for simplicity, we have assumed that $r(\omega)$ is independent of frequency. These simulations also assume a value of $s(\omega) = 1$, which we know to be correct only in the low frequency limit. However, its precise value at higher frequencies is unknown and is therefore a source of error in the noise reduction predictions. Finally, the slit height $2h$ in the expression for the tuned frequency $\omega_0 = \pi U/2h$ is adjusted by no more than 20% of the physical value $2h$ to give best fit to the frequency of maximum noise reduction. This slit height $2h$ may therefore be regarded as the effective slit height h_{eff} corresponding to the streamwise separation distance between the two effective centres of the sources at either ends of the slit.

Very good agreement is found over the entire frequency range with the measured noise reduction spectra by the simple model obtained by adjusting just the two parameters of ω_0 and $r(\omega)$ (where $\omega/\omega_0 \approx 1$), whilst assuming $s(\omega) = 1$. A second peak in the noise reduction spectra is also observed at a non-dimensional frequency of about 3 for the largest slit width w = 4.3 mm. This second peak is closer to 2.5 for the narrowest slit of 0.7 mm, suggesting that the effective distance is smaller than the physical distance in this case. Numerical studies are needed to understand the precise location of compact source regions and its frequency dependence.

The key to obtaining good levels of noise reduction by the use of these slitted profiles is to ensure that the source strengths at either ends of the slit are as equal as possible at the tuned frequency $\omega/\omega_0 = 1$. It is therefore important to understand how the optimum ratio of source strengths $r(\omega_0)$ varies with w. An estimate for $r(\omega_0)$ for any slitted geometry may be obtained from the value which provides best agreement between measured and predicted noise

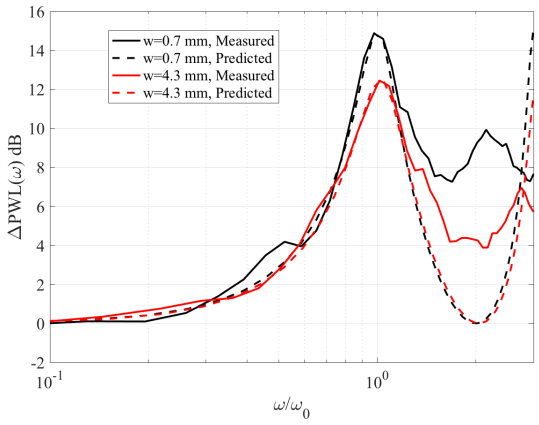

Fig. 11 Comparison between analytic and experimental noise reductions for two different slitted serrations of w =0.7, 4.3 mm at optimum conditions of a/w =6.8, 5.7, at a fixed, $2h/c_0$ =0.33 ($h_{eff}/2h = 0.8, 0.91$) at jet velocity U=60 m/s.

reduction spectra.

We now consider the variation in source strength ratio $r(\omega)$ (blue line) and effective height $h_{eff}/2h$ (red line) with slit width, which we plot in Fig. 12 against slit width w. The results for 7 values of w at the optimum ratio of a/w identified in Table 2 are plotted. This figure suggests that $r(\omega)$ tends, from above, towards a minimum value of 1.4 as w decreases. This figure also suggests that $h_{eff}/2h$ tends towards 1 (i.e., towards geometric height) as the slit width w increases. This is consistent with the assumption that for the narrowest slits, the precise location of the sources are closer together than the actual slit height. However, for wider slits, the effective height is very similar as the actual height.

We emphasize that the estimates of $r(\omega)$ in Fig. 12 are only approximate values owing to the possibly erroneous assumption that $s(\omega)$=1 and that $r(\omega)$ is frequency independent. Additional sources of error are also introduced by the assumption that the sources are perfectly coherent. Nevertheless, Fig. 12 provides useful information about how to design slitted profiles for obtaining maximum noise reductions.

For a particular tuned frequency ω_0 and flow speed U, an approximate estimate for the slit height can be obtained from $h = \pi U/2\omega_0$. From Table 2 the optimum ratio a/w can be found, which is approximately close to 7. From Figure 12, the slit width w should be made as small as possible to ensure that the source strengths at either ends of the slits are equal as possible (assuming that $s(\omega) = 1$). Once w is chosen, the precise value of h_{eff} can be found from Figure 12.

C. Chopped peak: Two partially coherent sources of different source strengths

To predict the noise reduction due to the chopped peak serrations, Eq. 6 developed in section VI.A is again applied but with the important difference that the sources are only partially coherent due to their spanwise separation. Its noise reduction spectrum plotted in Fig. 2 shows a series of broad peaks over and above the general frequency trend

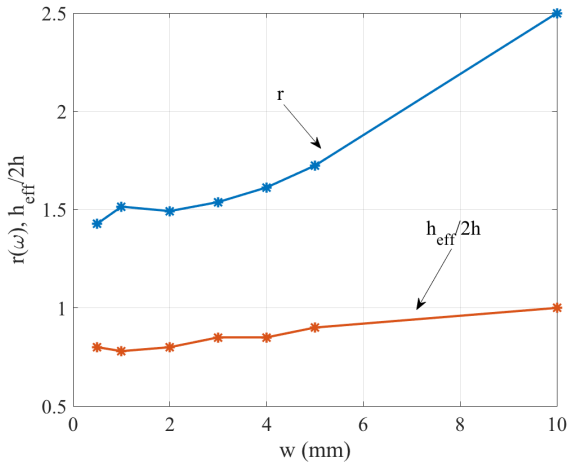

Fig. 12 Optimum source strength r and effective height h_{eff} versus w calculated from the measured data.

obtained with conventional single-wavelength serrations. The purpose of the model is to explain the reason for these additional peaks and not to provide an absolute noise prediction since the precise source strength distribution can only be determined by numerical methods.

As sketched in Fig. 1c the chopped-peak profile is completely defined by a chopped-peak width l_c/λ, a maximum peak-to-root distance $2h$ and a wavelength λ whose values investigated experimentally are listed in Table 1. Using this profile $x(y)$ in Eq. 6 and assuming uniform source strength along the leading edge, the noise prediction using this expression is plotted in Fig. 13 against $f(2h)/U$ and compared against the measured additional noise reduction spectra obtained by subtracting the noise spectrum due to the single wavelength serration. A significant discrepancy of about 5dB between the predicted and measured noise reductions is most likely due to the incorrect assumption regarding the source distribution. However, the peak frequencies in the noise reduction spectrum of $f(2h)/U = 0.81, 1.6, 2.5$ are well captured by the simple phase model. Note that these frequencies are roughly in the ratio 1:2:3, which differs considerably from the slit geometry whose peak frequencies are odd harmonics 1:3:5 etc. This finding suggests that additional noise reductions for this geometry arise from an enhanced source strength at the peak, whose distribution is in phase, interfering with the integrated response along the oblique edges.

D. Variable slit profiles: Multiple sources of different source strengths with partial coherence

The final geometry investigated in this paper comprises a series of narrow slits of varying heights, as sketched in Fig. 1e, in order to achieve noise reductions over a wider range of frequencies than previous geometries that are tuned to a particular frequency. This geometry is completely defined by the slit width a, distance between adjacent slits b, total height $2h$ and wavelength λ. The values of these parameters investigated experimentally above are listed in Table 1 and are h/c_0= 0.167, λ/c_0= 0.2, $d/\lambda = 0.066$ and $b/\lambda = 0.13$, and correspond to a geometry comprising six root sources and five peak sources per wavelength.

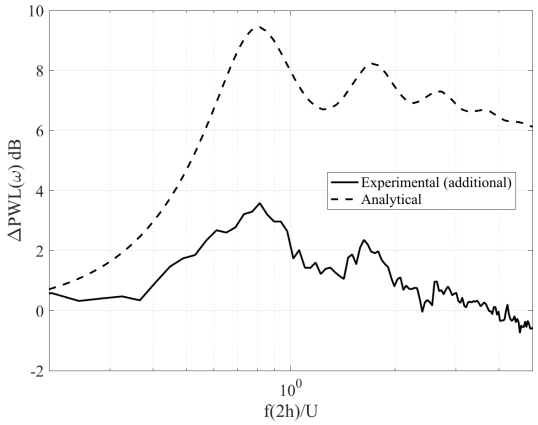

Fig. 13 Comparison between analytical and experimental additional noise reductions for Chopped-peak serrations for $l_c/\lambda = 0.33$, $2h/c_0 = 0.33$, $\lambda/c_0 = 0.1$ U=60 m/s.

The geometry $x(y)$ described above was input to the noise prediction model of Eq. 4. This prediction assumes two scenarios. The first assumes discrete sources of constant strength located at the six root locations only. The second prediction assumes discrete sources of constant strength at the six roots and five peaks. All sources are assumed to be partially coherent, similar to sinusoidal serration as discussed in section VI.A.

Figure 14 shows a comparison between the measured and the two predicted noise reduction spectra at a flow velocity of 60 m/s. The prediction assuming only root sources to match qualitatively the measured noise reduction spectrum in the low frequency range $f2h/U$ between 0.2 and 1. Clearly, the additional levels of noise reductions arise mostly from interference between the root sources, which are therefore dominant at these low frequencies. However, the additional peak at $f2h/U$ between 1 and 2 is not captured by assuming root sources alone. Once peak sources are included, this peak is now evident in the prediction, clearly indicating the role of both peak and root sources to the reduction in this higher frequency range.

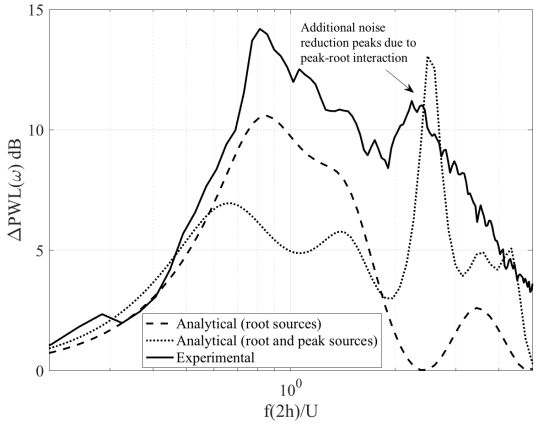

Fig. 14 Comparison between analytical and experimental additional noise reductions for Variable slit profiles of $\lambda/c_0 = 0.2$, $h/c_0 = 0.167$ at jet velocity U=60 m/s.

VII. Conclusion

This paper has proposed a number of leading edge profiles for the reduction of aerofoil interaction noise. Each of the five profiles investigated experimentally were shown to provide superior low frequency noise reductions compared to conventional single-wavelength serrations. These new profiles are characterized by having at least two dominant, highly coherent compact source regions per serration wavelength. High levels of destructive interference therefore occur at certain frequencies, unlike single-wavelength serrations which have only one dominant source at the serration root. A particular benefit of these new profiles, therefore, is that their low frequency performance is considerably enhanced through interference and source strength reduction compared with single wavelength profiles. Of all the profiles considered in this paper, introducing simple narrow slits into the aerofoil leading edge has been shown to provide the best low frequency noise reduction performance.

An optimum slit ratio 7 times narrower than the leading edge length has been identified as providing the greatest noise reductions. This paper has demonstrated noise reductions at a flow speed of 60m/s of almost 15dB over the microphone array compared with noise reductions of just 10dB for a conventional sinusoidal profile of the same overall amplitude.

Noise predictions obtained from the Wiener-Hopf solution were shown to be in poor agreement agreement with the experimental data for these optimum geometries except single-wavelength profile, which we believe is because it does not include the presence of secondary vorticity, which plays an important role in determining the acoustic source strength distribution. A simple analytical model is presented to understand the essential noise reduction mechanism. It is based on the hypothesis of sources distributed along the leading edge whose relative phase difference is determined by the different convection times required by eddies to arrive at the leading edge. A major drawback with the simple method is that the source distribution and its coherence must be known *a priori*.

This paper has demonstrated conclusively that single-wavelength or sawtooth leading edge profiles, that have been widely investigated in previous works, provide levels of noise reduction that are significantly inferior to those achievable by the new designs. Further work is needed to understand the factors that control the source strength distribution along the edge to optimize the leading edge profile further and enable the simple source model to be used as a predictive tool. Further refinement of the slitted profiles is also possible in that they may be rounder and avoid sharp corners as long as the source balance is not affected. Further work is needed to establish their performance in realistic flow situations, such as at incidence and high flow speeds where viscous effects may become an issue. Finally, more work is also needed to quantify the effect of slits on aerodynamic performance. Any degradation in aerodynamic performance must of course be balanced against the positive effects of reduced noise.

Acknowledgments

This work was partly supported by the EPSRC (EP/J007633/1) and by InnovateUK, HARMONY Programme ($GAn°101367$) (CP and PFJ). Further support came from EPSRC early career fellowship EP/P015980/1 (LJA). Rolls-Royce Plc is also acknowledged for the financial and technical support given.

Appendix

The far-field acoustic pressure due to a single frequency incident gust is given (in cylindrical coordinates centered on the leading edge, with the y-axis aligned with the aerofoil span) by

$$p(r,\theta,z) \sim i\sum_{n=-\infty}^{\infty}\left(\frac{k_1}{\beta^2}-w_n\cos\theta\right)\frac{e^{\pi i/4}}{\sqrt{\pi}}G_n^+(-w_n\cos\theta)E_n(-w_n\cos\theta) \times\cos\left(\frac{\theta}{2}\right)\frac{e^{iw_nr}}{\sqrt{r}}Z_n(-w_n\cos\theta,y)e^{-4iw_n\cos\theta hF(y)}. \tag{13}$$

Here, lengths are non-dimensionalised by the serration wavelength and velocities by the far-upstream mean flow. $F(y)$ denotes the serration geometry normalised such that $\max_y F = 0.25$ and $\min_y F = -0.25$. k_1 is the gust streamwise wavenumber, $w_n^2 = (\delta M)^2 - (k_2 + 2n\pi)^2$, with k_2 the spanwise gust wavenumber, and $\delta = k_1/\beta$, $\beta^2 = 1 - M^2$, for M the Mach number of the far-upstream flow.

Finally,

$$Z_n(\alpha,y) = e^{i\alpha cF(y)}e^{ik_2y+2n\pi iy}, \tag{14}$$

$$G_n^+(\alpha) = \frac{i}{\alpha+\delta}\frac{1}{\sqrt{-\delta-w_n}}, \tag{15}$$

and

$$E_n(\alpha) = \int_0^1 e^{4ik_1hF(\zeta)+ik_2\zeta}\overline{Z_n(\bar{\alpha},\zeta)}d\zeta, \tag{16}$$

where the overbar denotes complex conjugation.

To obtain the far-field acoustics for grid-generated turbulent flow, we integrate over a spanwise wavenumber spectrum, Φ^∞,

$$\mathrm{SPL} = 10\log_{10}\left(\int_{-\infty}^{\infty}|p^*|^2\Phi^{(\infty)}(k_1,k_2)dk_2\right) + \mathrm{SPL}_{\mathrm{TE}}, \tag{17}$$

where $\Phi^{(\infty)}(k_1,k_2)$ is the upstream Liepmann spectrum given by

$$\frac{3\overline{u^{*2}}\Lambda^{*2}}{4\pi}\frac{\Lambda^2(k_1^2+k_2^2)}{\left(1+\Lambda^2(k_1^2+k_2^3)\right)^{5/2}}, \tag{18}$$

where we have used * to denote a dimensional quantity. We also have added a contribution for trailing-edge noise, $\mathrm{SPL}_{\mathrm{TE}}$, which may be obtained from Amiet's formulation.

For full details in the derivation of this solution, see [25].

References

[1] Buck, S., Oerlemans, S., and Palo, S., "Experimental Validation of a Wind Turbine Turbulent Inflow Noise Prediction Code," *AIAA Journal*, Vol. 56(4), 2018, pp. 1495–1506.

[2] Howe, M., "Aerodynamic noise of a serrated trailing edge," *Journal of Fluids and Structures*, Vol. 5(1), 1991, pp. 33–45.

[3] Soderman, P., "Aerodynamic effects of leading-edge serrations on a two- dimensional airfoil," Tech. rep., NASA TM X-2643, 1972.

[4] Hersh, A., Soderman, P., and Hayden, R., "Investigation of acoustic effets of leading edge serrations on airfoils," *Journal of Aircraft*, Vol. 11(4), 1974, pp. 197–202.

[5] Roger, M., Schram, C., and De Santana, L., "Reduction of Airfoil Turbulence-Impingement Noise by Means of Leading-Edge Serrations and/or Porous Materials," *19th AIAA/CEAS Aeroacoustics Conference, AIAA 2013-2108*, 2013.

[6] Clair, V., Polacsek, C., Garrec, T. L., Reboul, G., Gruber., M., and Joseph, P., "Experimental and Numerical Investigation of Turbulence-Airfoil Noise Reduction Using Wavy Edges," *AIAA Journal*, Vol. 51(11), 2013, pp. 2695–2713.

[7] Lau, A. S., Haeri, S., and Kim, J. W., "The effect of wavy leading edges on aerofoil-gust interaction noise," *Journal of Sound and Vibration*, Vol. 332, 2013, pp. 6234–6253.

[8] Narayanan, S., Chaitanya, P., Haeri, S., Joseph, P., Kim, J. W., and Polacsek, C., "Airfoil noise reductions through leading edge serrations," *Physics of Fluids*, Vol. 27, No. 025109, 2015.

[9] Chong, T. P., Vathylakis, A., McEwen, A., Kemsley, F., Muhammad, C., and Siddiqi, S., "Aeroacoustic and Aerodynamics performance of an aerofoil subjected to sinusoidal leading edges," *21st AIAA/CEAS Aeroacoustics Conference, AIAA 2015-2200*, 2015.

[10] Lyu, B., Azarpeyvand, M., and Sinayoko, S., "Noise prediction for serrated leading-edges," *22nd AIAA/CEAS Aeroacoustics Conference, AIAA 2016-2740*, 2016.

[11] Kim, J., Haeri, S., and Joseph, P., "On the reduction of aerofoil-turbulence interaction noise associated with wavy leading edges," *Journal of Fluid Mechanics*, Vol. 792, 2016, pp. 526–552.

[12] Chaitanya, P., Joseph, P., Narayanan, S., Vanderwel, C., Turner, J., Kim, J. W., and Ganapathisubramani, B., "Performance and mechanism of sinusoidal leading edge serrations for the reduction of turbulence-aerofoil interaction noise," *Journal of Fluid Mechanics,*, Vol. 818, 2017, pp. 435–464. URL doi:10.1017/jfm.2016.95.

[13] Gea-Aguilera, F., Gill, J. R., Angland, D., and Zhang, X., "Wavy Leading Edge Airfoils Interacting with Anisotropic Turbulence Read More: https://arc.aiaa.org/doi/abs/10.2514/6.2017-3370," *23rd AIAA/CEAS Aeroacoustics Conference, AIAA 2017-3370*, 2017.

[14] Juknevičius, A., and Chong, T. P., "On the leading edge noise and aerodynamics of thin aerofoil subjected to the straight and curved serrations," *Journal of Sound and Vibration*, Vol. 425, 2018, pp. 324–343.

[15] G.Bampanis, M.Roger, D.Ragni, F.Avallone, and C.Teruna, "Airfoil-Turbulence Interaction Noise Source Identification and Reduction by Leading-Edge Serrations," *25th AIAA/CEAS Aeroacoustics Conference, AIAA 2019-2741*, 2019.

[16] Krömer, F., Renz, A., and Becker, S., "Experimental Investigation of the Sound Reduction by Leading-Edge Serrations in Axial Fans," *AIAA Journal*, Vol. 56(5), 2018, pp. 1–5.

[17] Biedermann, T. M., Czeckay, P., Geyer, T. F., Kameier, F., and Paschereit, C. O., "Effect of Inflow Conditions on the Noise Reduction Through Leading Edge Serrations," *AIAA Journal*, Vol. 57(7), 2019, pp. 1–6.

[18] Turner, J. M., and Kim, J. W., "Aeroacoustic source mechanisms of a wavy leading edge undergoing vortical disturbances," *Journal of Fluid Mechanics*, Vol. 811, 2017, pp. 582–611.

[19] Ayton, L., and Kim, J.-W., "An analytic solution for the noise generated by gust–aerofoil interaction for plates with serrated leading edges," *Journal of Fluid Mechanics,*, Vol. 853, 2018, pp. 515–536. URL doi:10.1017/jfm.2018.583.

[20] Huang, X., "Experiments on an elliptic circulation control aerofoil," *Journal of Fluid Mechanics*, Vol. 819, 2017, pp. 228–257.

[21] Casalino, D., Avallonea, F., Gonzalez-Martinoc, I., and Ragnia, D., "Aeroacoustic study of a wavy stator leading edge in a realistic fan/OGV stage," *Journal of Sound and Vibration*, Vol. 442(3), 2019, pp. 138–154.

[22] Chaitanya, P., Narayanan, S., Joseph, P., and Kim, J. W., "Leading edge serration geometries for significantly enhanced leading edge noise reductions," *22nd AIAA/CEAS Aeroacoustics Conference, AIAA 2016-2736*, 2016.

[23] Chaitanya, P., Joseph, P., Narayanan, S., and Kim, J. W., "Aerofoil broadband noise reductions through double-wavelength leading-edge serrations: a new control concept," *Journal of Fluid Mechanics,*, Vol. 855, 2018, pp. 131–151. URL doi:10.1017/jfm.2018.620.

[24] Chaitanya, P., and Joseph, P., "Slitted leading edge profiles for the reduction of turbulence-aerofoil interaction noise," *Journal of acoustical society of America*, Vol. 143(6), 2018, pp. 3494–3504.

[25] Ayton, L., and Chaitanya, P., "An analytical and experimental investigation of aerofoil-turbulence interaction noise for plates with spanwise-varying leading edges," *Journal of Fluid Mechanics,*, Vol. 865, 2019, pp. 137–168. URL doi:10.1017/jfm.2018.620.

[26] Turner, J., "Aerodynamic Noise from Undulated Leading Edge Aerofoils," Ph.D. thesis, University of Southampton, 2018.

[27] Cannard, M., Joseph, P., Kim, J.-W., and Chaitanya, P., "Slitted leading-edge profiles for the reduction of broadband interaction noise; physical mechanisms and performance," *25th AIAA/CEAS Aeroacoustics Conference, AIAA 2019-2511*, 2019.

[28] Chaitanya, P., Joseph, P., and Ayton, L., "On the superior performance of leading edge slits over serrations for the reduction of aerofoil interaction noise," *24th AIAA/CEAS Aeroacoustics Conference, AIAA 2018-3121*, 2018.

[29] Chong, T. P., Joseph, P., and Davies, P. O. A. L., "A parametric study of passive flow control for a short, high area ratio 90^{o} curved diffuser," *Journal of Fluids Engineering*, Vol. 130, No. 11, 2008, pp. 111104–12.

[30] Hinze, J., "0. 1975 Turbulence," , 1972.

[31] Amiet, R., "Acoustic radiation from an airfoil in a turbulent stream," *Journal of Sound and Vibration*, Vol. 41(4), 1975, pp. 407–420.

[32] Mish, P. F., "An Experimental Investigation of Unsteady Surface Pressure on Single and Multiple Airfoils," Ph.D. thesis, Virginia Polytechnic Institute and State University, 2003.